Quantitative insight into dislocation nucleation from high-temperature nanoindentation experiments

C. A. SCHUH*, J. K. MASON AND A. C. LUND

Department of Materials Science and Engineering, Massachusetts Institute of Technology, 77 Massachusetts Avenue, Cambridge, Massachusetts 02139, USA
*e-mail: schuh@mit.edu

Published online: 17 July 2005; doi:10.1038/nmat1429

Nanoindentation has become ubiquitous for the measurement of mechanical properties at ever-decreasing scales of interest, including some studies that have explored the atomic-level origins of plasticity in perfect crystals. With substantial guidance from atomistic simulations, the onset of plasticity during nanoindentation is now widely believed to be associated with homogeneous dislocation nucleation. However, to date there has been no compelling quantitative experimental support for the atomic-scale mechanisms predicted by atomistic simulations. Our purpose here is to significantly advance the quantitative potential of nanoindentation experiments for the study of dislocation nucleation. This is accomplished through the development and application of high-temperature nanoindentation testing, and the introduction of statistical methods to quantitatively evaluate data. The combined use of these techniques suggests an unexpected picture of incipient plasticity that involves heterogeneous nucleation sites, and which has not been anticipated by atomistic simulations.

Our understanding of the elastic–plastic transition on the nanoscale has been dramatically advanced by nanoindentation studies of plastic yielding in dislocation-free crystalline regions beneath the indenter tip[1–19]. Experimentally, the problem of 'incipient plasticity' is studied through the examination of indentation load–displacement (P–h) curves, acquired when a stiff indenter is brought into mechanical contact with a clean crystalline surface. A typical P–h response of this kind is shown for a specimen of (110)-oriented platinum in Fig. 1a. With increasing load there is initially an elastic deflection, and plastic deformation is typically found to initiate with a discrete burst of displacement, as the indenter tip 'pops' into the specimen[1,2,5,13–15,19,20].

Our current understanding of incipient plasticity and the first displacement burst seen in Fig. 1a is largely due to atomistic simulations, which have now been performed by a number of authors for nanoindentation of perfect metal crystals[3,4,6–11]. By directly observing the calculated atomic motions under the indenter, the first discontinuity in the P–h curve has been correlated with homogeneous dislocation nucleation, and further analysis has provided significant quantitative insights into this process[3,10,11]. This deep simulation-based understanding stands in stark contrast to the kind of information typically gleaned from nanoindentation experiments. Some authors have experimentally estimated the crystal strength at the first displacement burst[1,5,12–15,20,21], and recovered values of the order of the ideal shear strength; this would be in line with expectations for homogeneous dislocation nucleation. More direct experimental evidence of dislocation nucleation has been supplied by *in situ* electron microscopy for a special geometry specimen of aluminium[22,23] but, in general, there has not been any quantitative experimental input to the problem. In what follows, we illustrate how a capability in high-temperature nanoindentation, coupled with a statistical method of analysis, can provide experimental input that is both quantitative and compelling.

Our approach to the incipient plasticity problem is based upon a simple observation that has been documented by a number of authors working in this area[5,16,18,24–27]: the initiation of the first displacement burst is stochastic. A series of nominally 'identical' nanoindentations on the same clean surface gives a significant spread of plastic yield points. Furthermore, there is apparently

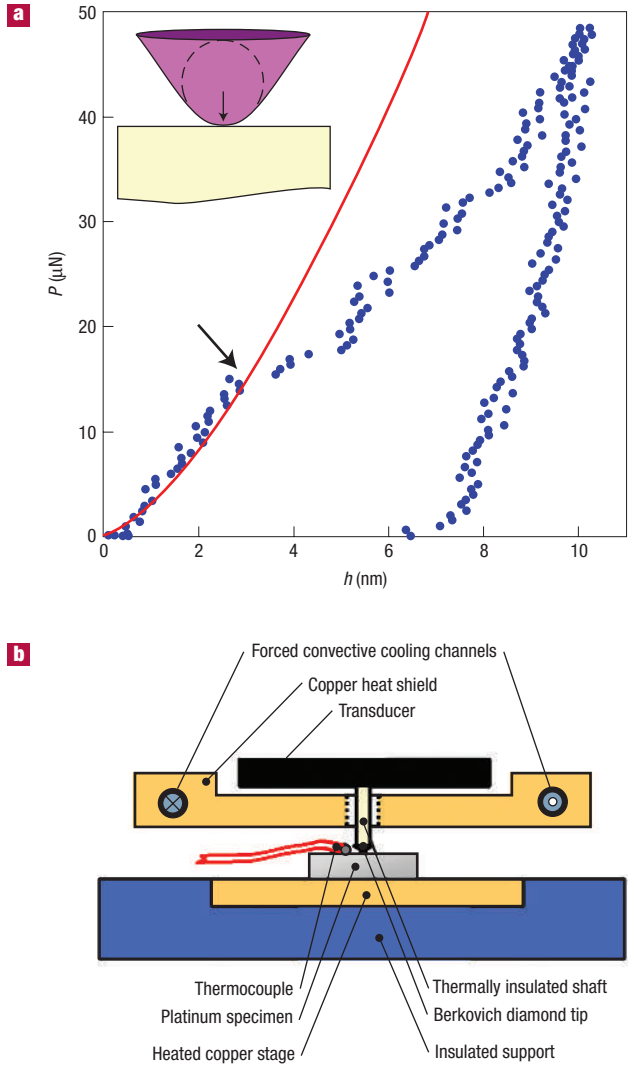

Figure 1 Nanoindentation at elevated temperatures. a, A typical load–displacement (*P–h*) curve for nanoindentation of (110)-oriented single-crystal platinum. The inset illustrates the geometry of the test, which in this case was conducted at 100 °C and $\dot{P} = 25\ \mu N\,s^{-1}$. The red curve illustrates the expected *P–h* curve for purely elastic loading, and the experimental data depart from this curve at a displacement burst (black arrow). **b**, A schematic representation of the experimental apparatus used in the present work, incorporating a heating stage and peripheral thermal-management equipment.

a subtle time or rate dependence to the incipient plasticity problem[1,16,18,24,27–30], although it has not received much detailed attention. In our opinion, these observations point to a significant contribution of thermal energy to the onset of plasticity at the nanoscale. We imagine that there is a local, kinetically limiting process that takes place under the indenter (for example, the nucleation of a dislocation) that requires an activation energy ε. This energy barrier could be reduced through the mechanical work of indentation, or may be overcome by an appropriate thermal fluctuation, or a combination of both. The probability of such an event in a given volume of material is written as

$$\dot{n} = \dot{n}_0 \cdot \exp\left(-\frac{\varepsilon - \sigma V}{kT}\right), \qquad (1)$$

where the attempt frequency for the event is $\dot{n}_0$ per unit volume, the mechanical work is equal to a stress σ acting on an activation volume V, and the thermal energy is Boltzmann's constant k multiplied by temperature T.

Later in this article we will develop in more detail the way in which equation (1) can be applied to understand incipient plasticity experiments. For the moment, however, the main point is that the atomic-level events that occur beneath the indenter are probabilistic, and the probability function can be changed by altering the conditions of the nanoindentation test. In particular, we note that extraction of the activation energy ε through equation (1) requires that nanoindentation experiments be performed at multiple temperatures.

Nanoindentation has historically been principally a room-temperature technique, owing to a combination of delicate actuation and sensing devices and severe sensitivity to thermal drift. Although some authors have performed nanoindentation experiments at non-ambient temperatures in the past[29–37], it is only recently that we have reported the ability to perform tests up to 200 °C with the extreme resolution required to observe and measure the displacement burst associated with incipient plasticity[38]. Our technique is based on relatively straightforward modifications to a commercial nanoindenter (see Methods and Fig. 1b), and in our latest unpublished work we have acquired sound *P–h* data at temperatures up to 410 °C.

In the current work, we have used high-temperature nanoindentation to study the first displacement burst on loading, and Fig. 2a illustrates some typical *P–h* curves that we acquired at 25, 100 and 200 °C on a clean (110)-oriented surface of single-crystal platinum. The results at any of these temperatures are qualitatively similar, and the difference in the position of the displacement burst from one temperature to another is rather subtle; qualitatively, it is difficult to observe any strong effect of temperature by comparing only individual *P–h* curves. However, when a statistical approach is taken, differences from one temperature to the next are clearly discernible, as illustrated in Fig. 2b. This figure plots the cumulative fraction, f, of displacement burst loads for three separate series of more than 130 'identical' indentations each. These data were acquired on the same surface of (110)-oriented platinum, with the same constant loading rate, $\dot{P} = 25\ \mu N\,s^{-1}$, but at three different test temperatures. It can be seen that temperature changes lead to a significant shift in the population of plastic yield loads, with higher test temperatures promoting earlier displacement bursts; this result is in line with the expectations of equation (1), as increased thermal energy lowers the required mechanical activation to promote yield. In a similar vein, we find that the yield-point distribution can also shift by virtue of changes in the indentation loading rate. This is illustrated in Fig. 2c for three different rates, all at a constant test temperature of 100 °C. In this case we see that slower indentations lead to earlier yield; the increased time-at-load allows more opportunity for a critical thermal fluctuation to occur.

The observations in Fig. 2 are in line with intuition for a statistical process such as that described by equation (1), but it remains an open question how the data and probability function can be quantitatively linked; it is our purpose in what follows to propose a framework for such an analysis. We begin by noting that equation (1) gives a displacement burst rate for a volume element of material under a constant stress state, but the stress field under a nanoindentation is a strong function of position. Therefore, the global rate at which displacement bursts would occur ($\dot{N}$) is found by integrating over the volume of the indented material near the contact region (Ω):

$$\dot{N} = \dot{n}_0 \cdot \exp\left(-\frac{\varepsilon}{kT}\right) \cdot \int_{\Omega}\int\int \exp\left(\frac{\sigma V}{kT}\right) d\Omega. \qquad (2)$$

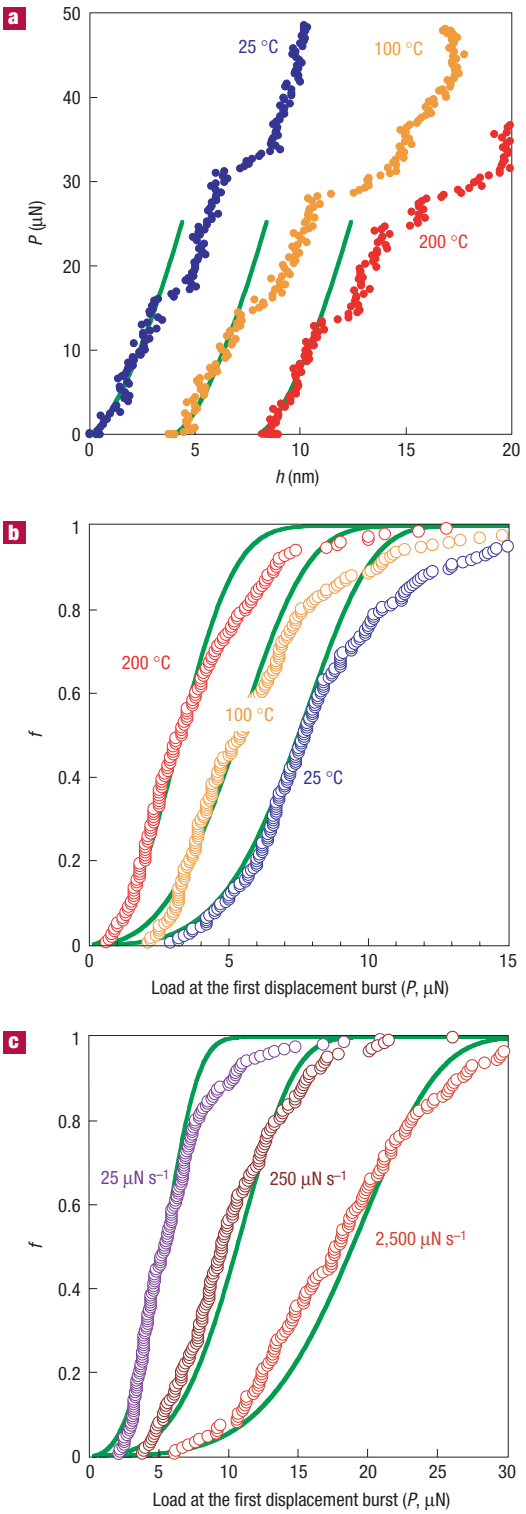

Figure 2 Statistics of the first displacement burst. a, Typical *P*–*h* curves measured upon loading at the three test temperatures, all at a constant loading rate of $\dot{P} = 250\ \mu\mathrm{N\,s^{-1}}$. The noise level in these curves is unaffected by temperature when proper test methods are used, and the initial part of the curve matches the expectations of hertzian elastic contact theory (green lines). **b**, The cumulative distribution of the load at the first displacement burst with $\dot{P} = 25\ \mu\mathrm{N\,s^{-1}}$, which is seen to have a significant temperature dependence as well as **c**, a significant rate dependence. The experimental data sets (shown as points), as well as the measured temperature dependence and rate dependence, are well captured by the statistics of thermal activation through equations (1)–(3), as illustrated by the solid green lines.

The evaluation of this integral requires not only that we know which terms from the full stress tensor constitute σ, but also that we know how stress changes with position beneath the indenter. The current understanding of incipient plasticity during nanoindentation is that the displacement burst corresponds to the nucleation of at least one dislocation, which occurs primarily due to the action of a shear stress, τ. Therefore, we take as our first approximation to this problem that $\sigma = \tau$. The advantage of this approximation is that τ is known analytically as a function of position beneath an elastic (hertzian) contact[39], and the integral in equation (2) can be readily evaluated for this case (more details of this evaluation are given in Methods).

Equation (2) gives the rate at which displacement bursts will occur under an indentation for fixed conditions. It is straightforward to link this rate equation to the cumulative statistics that we acquire by experiment as[27]

$$f = 1 - \exp\left(-\int_0^t \dot{N}\,\mathrm{d}t\right), \qquad (3)$$

where t is time, and the integral runs from the beginning of the indentation to the current time under consideration. After evaluation (see the Methods section for details), equation (3) gives the form of the cumulative displacement burst load distributions such as we acquire from experiment (see Fig. 2). Furthermore, the form of the predicted curves depends upon both temperature (through the kT term in equation (1)) and loading rate (through the time-integral in equation (3)). Because we have no *a priori* knowledge of the values of the attempt frequency, the activation volume, or the activation energy that control incipient plasticity, we treat all three of these parameters as adjustable, and fit equation (3) to the experimental data. In the present case we have performed such fitting over all of the data sets shown in Fig. 2, as well as nine additional sets of data for combinations of temperature and loading rate not shown. A total of 2,183 individual indentations were used in this analysis.

The results of the fitting procedure are shown by the green solid lines superimposed on the experimental data in Fig. 2. From these graphs we see that our statistical interpretation of incipient plasticity captures the proper sigmoidal trend of the curves, as well as the shifts in the cumulative distributions that arise from either temperature or loading rate changes. Furthermore, this analysis yields quantitative estimates for the activation energy, activation volume and attempt frequency underlying incipient plasticity. In the present case we obtain an activation volume of $V \approx 10.2\ \text{Å}^3$, an activation energy of $\varepsilon \approx 0.28$ eV, and an attempt frequency of $\dot{n}_0 \approx 1.8 \times 10^{25}\ \mathrm{s^{-1}m^{-3}}$. We emphasize that whereas activation volumes of this same order have been estimated previously from displacement burst experiments[18,27], our new capability in elevated-temperature testing allows the measurement of ε and $\dot{n}_0$ for the first time here.

According to the homogeneous dislocation nucleation picture of incipient plasticity, the first displacement burst is controlled by a cooperative process of atomic motion to form a critical-sized dislocation loop. Simulations have shown that small sub-critical fluctuations may occur before the formation of a stable dislocation loop, and that the nucleation event can in fact be traced back to a specific initial thermal-fluctuation site[18]. However, the critical event necessarily requires many atoms moving together, so the activation volume for homogeneous loop nucleation is expected to be very large, comprising many atomic volumes[7,14,16,34,40]. Similarly, the activation energy should be reflective of many bond breakages, of the order of several electron-volts. Finally, the attempt frequency for homogeneous nucleation would be of the order of the product of the Debye frequency and the number of atoms per cubic metre in platinum, roughly $10^{41}\ \mathrm{s^{-1}m^{-3}}$.

On comparing our experimentally extracted activation parameters with those described above for homogeneous dislocation nucleation, we see that the experimental values of ε, V and $\dot{n}_0$ are all strikingly small. With an activation volume somewhat smaller than the cubed Burger's vector ($V \approx 0.5\ b^3$), an activation energy ($\varepsilon \approx 0.28$ eV) below that for point-defect migration in platinum[41] (~1.3 eV), and an attempt frequency low by more than ten orders of magnitude, we judge it quite unlikely that the present data correspond to the homogeneous nucleation of a dislocation loop beneath the nanoindenter. Furthermore, the numerical values presented above are extremely robust; as described in more detail in the Methods section, we have used numerous procedures and mathematical variations of the form of equation (1) in our fitting procedure, and in every case we obtain activation parameters of this same order. These data clearly suggest a new picture of incipient plasticity: the first displacement burst during nanoindentation is rate limited by a low-energy process on the scale of a point defect, and can occur only at a small fraction of atomic sites.

Although it is impossible from the present analysis to conclusively infer details of the atomic motions under the nanoindenter, it is clear from the above discussion that a process of heterogeneous dislocation nucleation is required. With this in mind, we can envisage a number of potential atomic-scale mechanisms that control incipient plasticity. For example, vacancies may be involved: (i) a critical dislocation loop could grow from a sub-critical fluctuation through a process of climb by vacancy absorption[18]; (ii) dislocations could nucleate at a pre-existing vacancy or vacancy cluster[42]. The measured activation volume (~0.5 b^3) for the initial displacement burst is of the order of a vacancy volume (~0.67 b^3, ref. 41) after allowing for the effects of hydrostatic pressure under the indenter and lattice relaxation into the vacancy. However, the measured activation energy is only about one-quarter of that required for a vacancy to migrate in the bulk, and because dislocation climb is rate limited by vacancy migration, we view mechanism (i) as relatively unlikely compared with mechanism (ii).

It is also possible that incipient plasticity is controlled by the presence of other heterogeneous nucleation sites: (iii) dislocation sources could operate from stress concentrations at surface asperities or irregularities[40,43]; (iv) the displacement burst may correspond to a source activation event stemming from one or more dislocations present beneath the indenter; the pre-existing dislocations could perhaps be introduced earlier through process (iii) above. Both mechanisms (iii) and (iv) are energetically plausible, as dislocation source activation commonly has an activation energy of the order ~0.5 eV in face-centred-cubic metals[44]. However, in these cases it is unclear why the activation volume would have the low value we have measured.

The full details of the critical event character, and its variation from one material to another, will certainly require additional investigation. It is also possible that several of the above mechanisms may all be active in a given set of experiments; this may explain why the experimental data and model in Fig. 2 do not exactly match at the tails of the curves. In any event, our findings indicate that heterogeneous mechanisms of dislocation nucleation should be the focus of future incipient plasticity studies.

Before concluding, it is useful to discuss the stresses involved in dislocation nucleation. In our statistical framework, the athermal shear yield stress for an average volume of platinum is found as $\tau = \varepsilon/V \approx 4.4$ GPa. This large value is approaching the magnitudes measured by other researchers using nanoindentation[1,5,12–15,20,21], who based their calculation on the maximum shear stress given by the hertzian contact model. However, the present value is marginally lower than the ideal shear strength of defect-free platinum (~5.3 GPa, ref. 45). Although these estimates of ideal shear yield stress are approximate at best, the difference here could be reflective of the proposed heterogeneous nature of the first displacement burst, which would be expected to occur at lower stresses than those required for homogeneous nucleation from a perfect crystal.

The findings we have presented above point to a critical need for atomistic simulations that involve realistic distributions of point defects beneath a nanoindenter. They also may offer new insights into the effects of size scale on plasticity, and the so-called indentation size effect, which creates difficulties in extracting bulk mechanical properties from nanoindentation data. In particular, the transition from atomistic (nucleation-dominated) deformation to continuum-level plasticity may be dependent upon the details of the nucleation mechanism.

METHODS

EXPERIMENTAL MATERIAL

The experimental material was a (110)-oriented Pt single crystal of 99.999% purity from Goodfellow (Berwin, Pennsylvania) which was chosen for its lack of a native oxide layer at ambient and higher temperatures. The specimen was polished to r.m.s. roughness of <1 nm through a process of mechanical polishing, followed by electropolishing in an aqueous solution of HCl and NaCl.

ELEVATED-TEMPERATURE NANOINDENTATION

Instrumented nanoindentation experiments were performed using a Triboindenter (from Hysitron, Minneapolis, Minnesota) equipped with a commercial heating stage customized for the present purposes. This system allowed for conductive heating of the specimen to test temperatures of 100 and 200 °C (in addition to room-temperature experiments), while shielding the displacement transducer from the heat source with a cooled copper fixture (see Fig. 1b). The diamond indenter was mounted to a shaft with low thermal conductivity, and had a Berkovich pyramidal geometry that was blunted into a roughly spherical tip of radius ~150 nm. For the indentations described here only the spherical portion of the tip is relevant. The temperature was monitored and controlled using a J-type thermocouple in direct contact with the Pt specimen, and indentations were selectively placed within 2 mm of the thermocouple probe tip, and no closer than 5 μm to one another. Before the indentation experiments, the tip was brought into contact with the specimen surface at a very light load of ~2 μN, and the entire system was allowed to equilibrate thermally for more than an hour; therefore the tip and specimen were both at the same temperature during the nanoindentation experiments. For all subsequent indentations performed at the same temperature, the tip was maintained in contact with the specimen surface to promote thermal stability, and moved from one location to the next while maintaining the set-point load of 2 μN. Using a separate thermocouple behind the heat shield, we have verified that the transducer did not see elevated temperatures even while the sample was maintained within ±0.3 K of the set-point. Provided that the system was allowed to equilibrate (with the tip in contact) for more than about an hour, we found that thermal drift became essentially negligible and the natural resolution of the instrument could be maintained without significant additional noise. The typical noise levels are reflected in the P–h curves of Fig. 2a, which are similar at all test temperatures. Further details of our procedures, including detailed measurements of thermal drift and noise, will be published separately.

The first displacement burst was identified by comparing the ideal elastic hertzian P–h curve with the experimental data, and identifying the first point of departure. In every case this was correlated with a horizontal (constant P) travel of the indenter tip (see Figs 1 and 2a). In some cases the indentation loads were below the first displacement burst, and in these cases the loading and unloading curves fell on top of one another, with no residual plastic indentation depth recorded. *In situ* contact-mode imaging of the indented area after such an experiment revealed no residual impression, verifying that the contact was purely elastic.

EVALUATION OF EQUATIONS (1)–(3)

The unknowns in equations (1)–(3) are the fitting parameters ε, V and $\dot{n}_0$, as well as the biasing stress term, σ. The incipient plasticity problem describes the elastic–plastic transition so an elastic contact model is appropriate for evaluating σ, and here we use the complete solution to the hertzian contact problem as laid out in ref. 39. The indenter tip is taken as spherical with a radius of 150 nm, as measured by fitting P–h curves on known standard materials (see, for example, ref. 27). The hertzian contact solution gives the value of all the terms in the stress tensor at every point beneath the indenter, and the local isostatic pressure p and maximum shear stress τ are easily evaluated for a known applied load. The elastic properties of the diamond indenter and platinum substrate are also required in this evaluation, and here we have used the temperature-dependent elastic moduli; the temperature effect is negligible for the particular temperatures studied in this work.

The volume integral in equation (2) is evaluated in the cylindrical coordinates of the Hertz problem. Because the integral is unbounded at infinite distances from the contact, a physically reasonable cutoff distance is required. We have performed the integration out to four contact radii, where the local stress values have dropped by a factor of ~10, and where it is extremely unlikely that any of the stress-biased events we are concerned with occur. Reasonable changes in the distance of integration do not substantially influence the results reported herein. Because of the time-integral in equation (3), the stress history of the specimen is also required (that is, σ as a function of t), and this is related to the loading rate applied during testing ($\dot{P}$) by means of the Hertz model. These mathematical manipulations have all been performed numerically in the present work. The fitting of equation (3) to experimental data was accomplished using an iterative procedure to minimize the squared error between prediction and data.

As noted in the text, we have performed the fitting procedure described here in many ways. The stress term σ was evaluated for shear-biased processes, pressure-biased processes, coupled shear-plus-pressure biases in various combinations (that is, using a stress function $\sigma = \tau - \alpha p$ with p the hydrostatic pressure and the coefficient α ranging from zero to one), and even incorporating terms for pressure-gradient energies, as might be relevant for vacancy-migration processes. We have also considered locally resolved values of the shear stress (cognizant of the crystal symmetry and the slip systems in face-centred-cubic platinum) in some evaluations. The details of all of these evaluations will be reported in more detail in a future publication, but the main result reported here is found to be essentially unchanged for any of these procedures. The activation volume and energy obtained with any of these kinetic models is always of the same order as the values presented in the text. The attempt frequency remained within the same range as that presented in the text, but was sensitive to small changes in the activation volume and energy, as described elsewhere[18].

Received 16 March 2005; accepted 17 May 2005; published 17 July 2005.

References

1. Gerberich, W. W., Venkataraman, S. K., Huang, H., Harvey, S. E. & Kohlstedt, D. L. The injection of plasticity by millinewton contacts. *Acta Metall. Mater.* **43**, 1569–1576 (1995).
2. Gerberich, W. W., Nelson, J. C., Lilleodden, E. T., Anderson, P. & Wyrobek, J. T. Indentation induced dislocation nucleation: The initial yield point. *Acta Mater.* **44**, 3585–3598 (1996).
3. Li, J., Van-Vliet, K. J., Zhu, T., Yip, S. & Suresh, S. Atomistic mechanisms governing elastic limit and incipient plasticity in crystals. *Nature* **418**, 307–310 (2002).
4. Fago, M., Hayes, R. L., Carter, E. A. & Ortiz, M. Density-functional-theory-based local quasicontinuum method: Prediction of dislocation nucleation. *Phys. Rev. B* **70**, 100102 (2004).
5. Suresh, S., Nieh, T. G. & Choi, B. W. Nano-indentation of copper thin films on silicon substrates. *Scripta Mater.* **41**, 951–957 (1999).
6. Knap, J. & Ortiz, M. Effect of indenter-radius size on Au(001) nanoindentation. *Phys. Rev. Lett.* **90**, 226102 (2003).
7. Kelchner, C. L., Plimpton, S. J. & Hamilton, J. C. Dislocation nucleation and defect structure during surface indentation. *Phys. Rev. B* **58**, 11085 (1998).
8. de la Fuente, O. R. *et al*. Dislocation emission around nanoindentations on a (001) fcc metal surface studied by scanning tunneling microscopy and atomistic simulations. *Phys. Rev. Lett.* **88**, 036101 (2002).
9. Lilleodden, E. T., Zimmerman, J. A., Foiles, S. M. & Nix, W. D. Atomistic simulations of elastic deformation and dislocation nucleation during nanoindentation. *J. Mech. Phys. Solids* **51**, 901–920 (2003).
10. Miller, R. E. & Acharya, A. A stress-gradient based criterion for dislocation nucleation in crystals. *J. Mech. Phys. Solids* **52**, 1507–1525 (2004).
11. Zhu, T. *et al*. Predictive modeling of nanoindentation-induced homogeneous dislocation nucleation in copper. *J. Mech. Phys. Solids* **52**, 691–724 (2004).
12. Corcoran, S. G., Colton, R. J., Lilleodden, E. T. & Gerberich, W. W. Anomalous plastic deformation at surfaces: Nanoindentation of gold single crystals. *Phys. Rev. B* **55**, R16057–R16060 (1997).
13. Kiely, J. D. & Houston, J. E. Nanomechanical properties of Au (111), (001), and (110) surfaces. *Phys. Rev. B* **57**, 12588–12594 (1998).
14. Michalske, T. A. & Houston, J. E. Dislocation nucleation at nano-scale contacts. *Acta Mater.* **46**, 391–396 (1998).
15. Gouldstone, A., Koh, H. -J., Zeng, K. -Y., Giannakopoulos, A. E. & Suresh, S. Discrete and continuous deformation during nanoindentation of thin films. *Acta Mater.* **48**, 2277–2295 (2000).
16. Chiu, Y. L. & Ngan, A. H. W. Time-dependent characteristics of incipient plasticity in nanoindentation of a Ni_3Al single crystal. *Acta Mater.* **50**, 1599–1611 (2002).
17. Wo, P. C. & Ngan, A. H. W. Incipient plasticity during nano-scratch in Ni_3Al. *Phil. Mag.* **84**, 3145–3157 (2004).
18. Wo, P. C., Zuo, L. & Ngan, A. H. W. Time-dependent incipient plasticity in Ni_3Al as observed in nanoindentation. *J. Mater. Res.* **20**, 489–495 (2005).
19. Page, T. F., Oliver, W. C. & McHargue, C. J. The deformation behavior of ceramic crystals subjected to very low load (nano)indentations. *J. Mater. Res.* **7**, 450–473 (1992).
20. Gane, N. & Bowden, F. P. Microdeformation of solids. *J. Appl. Phys.* **39**, 1432–1435 (1968).
21. Chiu, Y. L. & Ngan, A. H. W. A TEM investigation on indentation plastic zones in Ni_3Al (Cr, b) single crystals. *Acta Mater.* **50**, 2677–2691 (2002).
22. Minor, A. M., Morris, J. W. & Stach, E. A. Quantitative in situ nanoindentation in an electron microscope. *Appl. Phys. Lett.* **79**, 1625–1627 (2001).
23. Minor, A. M., Lilleodden, E. T., Stach, E. A. & Morris, J. W. Direct observations of incipient plasticity during nanoindentation of Al. *J. Mater. Res.* **19**, 176–182 (2004).
24. Wang, W., Jiang, C. B. & Lu, K. Deformation behavior of Ni_3Al single crystals during nanoindentation. *Acta Mater.* **51**, 6169–6180 (2003).
25. Mann, A. B. & Pethica, J. B. The effect of tip momentum on the contact stiffness and yielding during nanoindentation testing. *Phil. Mag. A* **79**, 577–592 (1999).
26. Shibutani, Y. & Koyama, A. Surface roughness effects on the displacement bursts observed in nanoindentation. *J. Mater. Res.* **19**, 183–188 (2004).
27. Schuh, C. A. & Lund, A. C. Application of nucleation theory to the rate dependence of incipient plasticity during nanoindentation. *J. Mater. Res.* **19**, 2152–2158 (2004).
28. Chinh, N. Q., Horváth, G., Kovács, Z. & Lendvai, J. Characterization of plastic instability steps occurring in depth-sensing indentation tests. *Mater. Sci. Eng. A* **324**, 219–224 (2002).
29. Syed-Asif, S. A. & Pethica, J. B. Nanoindentation creep of single-crystal tungsten and gallium arsenide. *Phil. Mag. A* **76**, 1105–1118 (1997).
30. Kramer, D. E., Yoder, K. B. & Gerberich, W. W. Surface constrained plasticity: Oxide rupture and the yield point process. *Phil. Mag. A* **81**, 2033–2058 (2001).
31. Volinsky, A. A., Moody, N. R. & Gerberich, W. W. Nanoindentation of Au and Pt/Cu thin films at elevated temperatures. *J. Mater. Res.* **19**, 2650–2657 (2004).
32. Lucas, B. N. & Oliver, W. C. Time dependent indentation testing at non-ambient temperatures utilizing the high temperature mechanical properties microprobe. *Mater. Res. Soc. Symp. Proc.* **356**, 645–650 (1995).
33. Lucas, B. N. & Oliver, W. C. Indentation power-law creep of high-purity indium. *Metall. Mater. Trans. A* **30**, 601–610 (1999).
34. Bahr, D. F., Wilson, D. E. & Crowson, D. A. Energy considerations regarding yield points during indentation. *J. Mater. Res.* **14**, 2269–2275 (1999).
35. Beake, B. D. & Smith, J. F. High-temperature nanoindentation testing of fused silica and other materials. *Phil. Mag. A* **82**, 2179–2186 (2002).
36. Xia, J., Li, C. X. & Dong, H. Hot-stage nano-characterizations of an iron aluminide. *Mater. Sci. Eng. A* **354**, 112–120 (2003).
37. Smith, J. F. & Zheng, S. High temperature nanoscale mechanical property measurements. *Surf. Eng.* **16**, 143–146 (2000).
38. Lund, A. C., Hodge, A. M. & Schuh, C. A. Incipient plasticity during nanoindentation at elevated temperatures. *Appl. Phys. Lett.* **85**, 1362–1364 (2004).
39. Fischer-Cripps, A. C. *Introduction to Contact Mechanics* (Springer, New York, 2000).
40. Hirth, J. P. & Lothe, J. *Theory of Dislocations* (Wiley, New York, 1982).
41. Wollenberger, H. in *Physical Metallurgy* (eds Cahn, R. W. & Haasen, P.) Ch. 18, 1621–1722 (North Holland, Amsterdam, 1996).
42. Seitz, F. On the formation of dislocations from vacancies. *Phys. Rev.* **79**, 890–891 (1950).
43. Zimmerman, J. A., Kelchner, C. L., Klein, P. A., Hamilton, J. C. & Foiles, S. M. Surface step effects on nanoindentation. *Phys. Rev. Lett.* **87**, 165507 (2001).
44. Conrad, H. in *High Strength Materials* (ed. Zackay, V. F.) Ch. 11, 436–509 (Wiley, New York, 1965).
45. Pokluda, J., Cerny, M., Sandera, P. & Sob, M. Calculations of theoretical strength: State of the art and history. *J. Comput.-Aided Mater. Design* **11**, 1–28 (2004).

Acknowledgements

This work was supported by the US Office of Naval Research; the views expressed herein are not endorsed by the sponsor. The collaborative support of Hysitron and the collaborative involvement of A. Hodge (Lawrence Livermore National Laboratory) are gratefully acknowledged.
Correspondence and requests for materials should be addressed to C.A.S.

Competing financial interests

The authors declare that they have no competing financial interests.